



**HAL**  
open science

## From Langmuir–Blodgett to Grafted Films

M. Gabaji, J. Médard, A. Hemmerle, J. Pinson, J. P Michel

► **To cite this version:**

M. Gabaji, J. Médard, A. Hemmerle, J. Pinson, J. P Michel. From Langmuir–Blodgett to Grafted Films. *Langmuir*, 2020, 36 (10), pp.2534-2542. 10.1021/acs.langmuir.9b03601 . hal-03224452

**HAL Id: hal-03224452**

**<https://hal.science/hal-03224452>**

Submitted on 11 May 2021

**HAL** is a multi-disciplinary open access archive for the deposit and dissemination of scientific research documents, whether they are published or not. The documents may come from teaching and research institutions in France or abroad, or from public or private research centers.

L'archive ouverte pluridisciplinaire **HAL**, est destinée au dépôt et à la diffusion de documents scientifiques de niveau recherche, publiés ou non, émanant des établissements d'enseignement et de recherche français ou étrangers, des laboratoires publics ou privés.



Distributed under a Creative Commons Attribution - NonCommercial - ShareAlike 4.0 International License

# From Langmuir Blodgett to Grafted Films

M. Gabaji <sup>a</sup>, J. Médard <sup>b</sup>, A. Hemmerle <sup>c</sup>, J. Pinson <sup>b,\*</sup>, J. P. Michel <sup>a,\*</sup>

<sup>a</sup> Université Paris-Saclay, CNRS, Institut Galien Paris Sud, 92296, Châtenay-Malabry, France.

<sup>b</sup> Université de Paris, ITODYS, CNRS, UMR 7086, 15 rue J-A de Baïf, F-75013 Paris, France

<sup>c</sup> Synchrotron SOLEIL, L'Orme des Merisiers, Saint Aubin, BP48, Gif-sur-Yvette CEDEX, France.

\*Corresponding author: [jean.pinson@univ-paris-diderot.fr](mailto:jean.pinson@univ-paris-diderot.fr) or [jean-philippe.michel@universite-paris-saclay.fr](mailto:jean-philippe.michel@universite-paris-saclay.fr)

A locally organized monolayer film strongly attached to a gold surface is obtained by transfer of a Langmuir Blodgett (LB) film of octadecylamine (ODA) or alcohol (ODOH) onto an *Au* surface and simultaneous oxidative electrografting of this film still in contact with the aqueous subphase. As opposed to LB films, these films resist ultrasonication and unlike electrografted films, they are organized monolayers by construction. They are characterized by AFM (Atomic Force Microscopy), water contact angle, ellipsometry, XPS (X-ray photoelectron spectroscopy) IRRAS (Infrared Reflection Absorption Spectroscopy) and GIXD (Grazing Incidence X-ray Diffraction).

## Introduction

The modification and functionalization of metallic surfaces with organic films is a subject of current interest in different fields: sensors, biomedical applications, organic electronics, energy storage... Several methods are available to achieve this goal: Langmuir-Blodgett (LB) films,<sup>1,2</sup> thiols on gold,<sup>3,4,5</sup> silanes<sup>6,7,8</sup> using chemisorption methods and/or the Langmuir method<sup>2,9,10</sup>, phosphonic acids<sup>11</sup> on oxidized surfaces and diazonium salts on metal oxidized or not.<sup>12,13</sup> These different methods can be classified according to the strength of attachment to the surface but also according to whether they provide organized or disorganized films. At one end of the

classification, Langmuir-Blodgett films are only physisorbed, that is they are weakly attached to the surfaces on which they are transferred but can be crystalline films;<sup>14,15,16,17</sup> at the other end one finds electrografted films that are strongly bonded to the surface, but are most often disordered multilayers.<sup>12</sup>

Before the LB transfer, long hydrocarbon chain amphiphiles can form organized monolayers at the air/water interface, such as octadecylamine (ODA). A thorough determination of the two-dimensional crystal structure of the Langmuir film can be achieved using grazing incidence X-ray diffraction (GIXD).<sup>18,19</sup> Numerous works reporting GIXD studies of Langmuir films made with silanes on water<sup>20,21</sup> or with long hydrocarbon chain amphiphiles,<sup>22</sup> such as  $C_nH_{2n+1}X$ , where X is a headgroup such as  $NH_2$ ,  $COOH$  or  $OH$ , demonstrated the existence of mesophases that possess partial orientational and translational order but also highly crystalline structures.<sup>17</sup>

The LB transfer of monolayers made of insoluble amphiphile molecules onto hydrophilic surfaces is usually performed at constant surface pressure that is maintained at a value adequate to keep the film in a relatively condensed state by constantly adjusting the film area. During the LB transfer, an angle exists between the monolayer and the substrate surface. This angle (by reference to the surface normal) depends on the amphiphile but may range from a few degrees to almost zero. The adhesion energy  $\Delta W$  between the monolayer and the substrate is then given by the Young-Dupre equation,<sup>23</sup>  $\Delta W = (1 - \cos \theta) \gamma_{\text{monolayer}}$ , with the subphase contact angle  $\theta$  and  $\gamma_{\text{monolayer}}$  the surface tension of the air/water interface in presence of the monolayer. For  $\theta$  values close to  $0^\circ$ , the energy of adhesion is therefore negligible with respect to energies associated with covalent bonds (for example  $154 \text{ kJ mol}^{-1}$  for an alkyl chain bonded to  $Au$ <sup>24</sup>). Indeed, physisorbed LB films are very fragile systems, very sensitive to mechanical perturbation.

The morphological characterization of self-assembled layers or LB films composed of long chain molecules has been extensively studied using scanning probe techniques, in particular for alkane-thiols on gold substrates. Atomic force and scanning tunneling microscopies (AFM and STM), as well as diffraction techniques, have been used to characterize a series of close-packed structures<sup>25,26,27</sup>. X-ray and neutron reflectivities have proven to be very powerful tools to study the structure of Langmuir or LB monolayers of long hydrocarbon chain amphiphiles.<sup>15,18,22,28</sup> They allow determination of scattering length density profiles along the film surface normal with a high resolution. Information about the lateral order within monolayers can be obtained

by GIXD.<sup>29,14</sup> Combined reflection and diffraction measurements have been conducted to reveal structural features as the pressure increases in the film.<sup>30</sup>

Electrografted films,<sup>31</sup> are obtained by electrochemical oxidation of amines<sup>32</sup>, carboxylates<sup>33</sup>, alcohols<sup>34</sup> or reduction<sup>12,35,36</sup> of diazonium salts,<sup>12</sup> and alkyl or aryl halides<sup>35,36</sup>. They result from the attack of very reactive radicals on the surface. The bond dissociation energies (BDE) of the *Metal*- and *Si*-aryl or alkyl films (obtained by reduction of diazonium salts or alkyl iodides) has been calculated by DFT methods,<sup>24,37,38</sup> and they vary from 100 to 293 kJ mol<sup>-1</sup> from *Au* to *Si* indicating a strong bonding of the organic film.<sup>37</sup> However the radicals react not only on the surface, but also with the first grafted group to provide strongly bonded multilayered disordered films.<sup>12</sup> Efforts have been made to limit the growth of the film in order to obtain monolayers. For example, with diazonium salts, the following procedures have been implemented: steric effects,<sup>39,40,41,42</sup> cleavage of multilayers,<sup>43</sup> use of ionic liquids<sup>44</sup> and radical traps<sup>45</sup> but none of them provided monolayers by construction, they only prevent the thickening of the film.

As concerns *Metal*-amine films the electrografting mechanism has been established,<sup>32</sup> but the formation of mono/multilayers has not been described in details. The surface concentrations of different films covalently bonded to surfaces have been measured (films obtained by oxidation of nitrobenzyl amine,<sup>33</sup> dopamine,<sup>46</sup> protected anilines and ethylenediamine<sup>47</sup>). Organic films obtained by electrografting amines have been used for flexible electronics,<sup>48</sup> analytical purposes,<sup>49</sup> modification of graphene oxide.<sup>50</sup> The formation of compact, organized strongly bonded monolayers films should be of interest to improve these applications, in particular as concerns biosensors.<sup>51,52,53</sup> Electrografting of alcohols has been much less investigated.<sup>54</sup> They have been grafted in aqueous acidic solution or in the presence of LiClO<sub>4</sub>, at quite positive potential (+ 1.85 V vs Ag wire for 1-octanol). The reaction mechanism has never been investigated in details and few applications have been developed.

The purpose of this paper is the construction of a covalently bound, organized monolayer of a long chain (C18) amine, such as octadecylamine (ODA), or alcohol (stearic alcohol ODOH) on *Au* surfaces by electrografting a Langmuir-Blodgett film during the transfer to the metallic surfaces (LB-eG process). The Langmuir film and the grafted one will be referred as ODA<sub>LB</sub> (the Langmuir Film on the water subphase), *Au*-ODA<sub>LB</sub> (the film LB-transferred on *Au*), *Au*-

ODA<sub>LB-G</sub> (the LB film grafted on Au) and Au-ODA<sub>G</sub> (the molecule directly electrografted on Au from the solution).

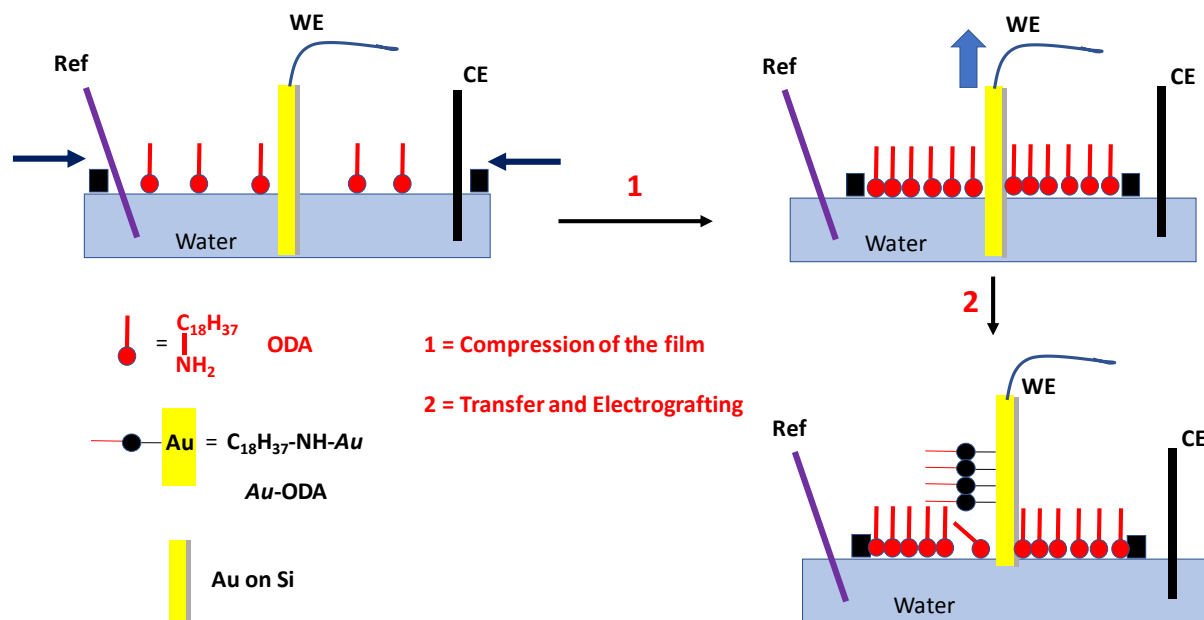


**Fig. 1:** Scheme describing the electrografting of a Langmuir Blodgett film. Ref: Reference electrode, WE: Working Electrode, CE: Counter Electrode.

## Experimental Section

*Substrates.* Gold (Au) coated silicon wafers obtained from the MPQ laboratory (Physics department, University Paris Diderot) with 100 nm thickness coating were cut into (1×1 cm<sup>2</sup>) pieces, cleaned with acidic piranha solution for 10 min and rinsed for 10 min in Milli-Q water.

*Equipment.*

The Langmuir equipment was a Langmuir trough KSV company (775.75 cm<sup>2</sup>, Biolin Scientific, Finland) enclosed into a Plexiglas box to limit surface contamination. The potentiostat used in the transfer experiments was from a Palm Sens 3. All the other experiments were performed with a Versastat 4 potentiostat/galvanostat/EIS from Princeton Applied Research analyzer with VersaStudio software.

*Formation of an electrografted film.* A gold plate was used as an anode in a 1mM ODA solution in DMF + 0.1M NBu<sub>4</sub>BF<sub>4</sub>, with a carbon counter electrode and a saturated calomel one. These three electrodes were connected to the potentiostat and chronoamperometry was started for 600s. Two different potentials were imposed + 0.85 V/SCE or + 1.40 V/SCE. After electrolysis the modified gold plates were rinsed in alcohol under sonication and characterized.

*Formation of a Langmuir-Blodgett film and simultaneous electrografting to Au surface.* A spreading organic solution was prepared by dissolving ODA (FW = 269.51 g/mol) or ODOH (FW = 270.49 g/mol) in chloroform/methanol (9/1 v/v) with a 3 μmol/mL concentration. The subphase was ultrapure water, purified with a milli-Q apparatus supplied by Millipore. The temperature of the subphase was maintained at 21°C. Its pH was 9, adjusted with a NaOH solution (pH 2 for ODOH adjusted with HCl). Before depositing organic solution, the gold substrate was previously immersed in the subphase and connected with the potentiostat. Prior to monolayer spreading, the subphase surface was cleaned by suction. Organic solutions of ODA or ODOH were spread onto water. The waiting time to allow a complete evaporation of the spreading solvent was 15 min before compression was started. The monolayer was compressed continuously at a constant rate of 5 Å<sup>2</sup>.molecule<sup>-1</sup>.min<sup>-1</sup>. The dipping speed and the surface pressure were kept respectively at 1 mm.min<sup>-1</sup> and 40 ± 0.2 mN/m. Under these conditions, ODA and ODOH monolayers were expected to be in a liquid condensed state. The Langmuir trough was equipped with saturated calomel electrode as a reference and carbon paper as counter electrode. Chronoamperometry at E = + 0.85V/SCE was started simultaneously with the transfer and stopped when the gold substrate was completely out of the aqueous solution.

*Characterization of the grafted film.*

*Atomic Force Microscopy experiments.* AFM experiments were performed using the Nanowizard 3 Ultra Speed from JPK Instruments (Berlin, Germany, [www.jpk.com](http://www.jpk.com)), installed on an air-buffered table coupled to a dynamic anti-vibration device, and enclosed in an acoustic box. Imaging of organic layers on Au substrates was performed in air in AC-HyperDrive® mode, with gold coated silicon cantilevers PPP-NCHAuD of 40 ± 10 N/m spring constant and 290 ± 5 kHz resonance frequency (Nanosensors, Neuchatel, Switzerland). The pyramid-shaped tips had a radius of curvature less than 10 nm. A free amplitude oscillation of 0.8 to 1 nm was chosen allowing a very high resolution of the imaged surface. Images were taken at scan rates of 1 Hz.

Image processing (flatten, plane fit, edge and hole detection) was performed with the JPK Data Processing software (JPK Instruments). At least three different areas of each sample were scanned and typical images were presented. Average values of height dimensions of holes were determined with all holes detected in the pictures.

*Infrared Spectra.* IRRAS spectra of the modified plates were recorded using a purged (low CO<sub>2</sub>, dry air) Jasco FT/IR-6100 Fourier transform infrared spectrometer equipped with an MCT (mercury-cadmium-telluride) detector. For each spectrum, 1000 scans were accumulated with a spectral resolution of 4 cm<sup>-1</sup>. The background recorded before each spectrum was that of a clean substrate.

*XPS Spectra.* XPS measurements were performed using a K-Alpha<sup>+</sup> system (ThermoFisher Scientific, East-Grinstead, UK) fitted with a micro-focused and monochromatic Al K $\alpha$  X-ray source (1486.6 eV, spot size: 400  $\mu$ m). The pass energy was set to 150 and 40 eV for the survey and the high resolution spectra, respectively. The spectra were calibrated against the C—C/C—H C1s component set at 285 eV. The chemical composition was determined by using the manufacturer sensitivity factors using Avantage software, version 5.9902. The spectra were calibrated against C1s set at 285 eV.

*Ellipsometry.* The thicknesses of the films on Au were measured with a Sentech SE400 monowavelength ellipsometer. The following refraction index values were taken for clean gold:  $n_s = 0.17$  and  $k_s = 3.31$ . These values were measured on cleaned surfaces before using the plates for grafting. The film thicknesses were determined from the same plates after modification, taking  $n_{org} = 1.46$ ,  $k_{org} = 0$  for the organic layer.

*Water Contact Angles.* They were measured with a Krüss DSA3 instrument. A drop (3  $\mu$ L) of Milli-Q water was automatically deposited on the top of the test sample placed in a horizontal position on the instrument stage. At least five measurements were made for each sample. The values of the contact angles were calculated by the tangent method using the Drop Shape Analysis software.

*Electrochemical Measurements.* All potentials are referred to the SCE electrode. The redox probes voltammograms were recorded on Au and Au-ODA<sub>LB-G</sub>, by delimitating a ring electrode on the plates by an adhesive plastic mask. A drop of the redox solution was deposited on this electrode. Reference and counter electrodes were positioned in the solution and voltammograms were recorded.

*GIXD measurements under synchrotron radiation.* X-ray scattering measurements were taken on the SIRIUS beamline at the SOLEIL Synchrotron (Saint Aubin, France)<sup>55</sup>. The scattering pattern was collected using a Pilatus 3 (Dectris, Switzerland) detector associated with Soller slit collimator (JJ-Xray, Denmark, resolution 0.06 deg) by scanning in the in-plane angle. The  $Q_{xy}$ - $Q_z$  images were generated by integrating horizontally the window defined by the Soller slit collimator on the original raw 2-D file of the detector to obtain the vertical distribution of the intensity.

Grazing incidence X-ray diffraction (GIXD) was performed on  $Au$ -ODA<sub>LB-G</sub> and  $Au$ -ODOH<sub>LB-G</sub> films at a fixed energy of 8 keV and used to obtain in-plane information about the molecular ordering on the gold surface. The scattered intensity was measured as a function of the angle  $2\theta$  between the incident and diffracted beams projected onto the horizontal plane. The angular positions  $2\theta$  were converted into the in-plane component of the scattering vectors  $Q_{xy} = (4\pi/\lambda) \sin 2\theta/2$ , and the vertical angles  $\theta_z$  to the out-of-plane component  $Q_z = (2\pi/\lambda) \sin \theta_z$ . The intensity map  $I(Q_{xy}, Q_z)$  was then integrated along  $Q_z$  yielding to  $Q_z$ -integrated spectrum  $I(Q_{xy})$ , or over  $Q_{xy}$  to obtain the Bragg rods  $I(Q_z)$ . Diffraction peaks were fitted along  $Q_{xy}$  with Lorentzian curves and along  $Q_z$  with sine cardinal functions. Their  $(Q_{xy}, Q_z)$  positions led to the structure of the two-dimensional lattice in real space. Their angular position  $2\theta_{hk}$ , corresponding to  $Q_{hk} = (4\pi/\lambda) \sin 2\theta_{hk}/2$ , yielded the distance  $d_{hk} = 2\pi/Q_{hk}$  for the two-dimensional (2D) lattice structure. They could be indexed by the two Miller indices  $h$  and  $k$  yielding the 2D unit cell. Full-width at half maximum (FWHM) values determined from the fits were used to determine the in-plane correlation length  $L$  using  $L = 2/\text{FWHM}$  in the case of Lorentzian shape peak<sup>56</sup>. The correlation length gives the spatial extension of the crystalline domains existing in the monolayer.

## Results

*LB transfer and electrografting.* In order to perform electrografting in a Langmuir trough, a gold or platinum plate is partly immersed in the trough and an electrical connection is made to this plate. In addition, a saturated calomel electrode (SCE) and a carbon paper counter electrode are introduced in the solution (Fig. SI-1 and Fig. 1). This permits to use the trough as an electrochemical cell. ODA is deposited on the surface of a pH 9 aqueous subphase from a spreading solution consisting of chloroform/methanol (3 mM). Compression is started after 15

minutes and surface pressure in the ODA film increased up to 40 mN/m (Fig. 2a). The LB transfer of the ODA<sub>LB</sub> film onto the Au surface is started simultaneously with chronoamperometry at E = + 0.85 V/SCE. This chronoamperometry stops when the plate is fully removed from the subphase. The plate is then rinsed under ultrasonication for 3 minutes in ethanol and dried under argon to give Au-ODA<sub>LB-G</sub>. Experiments using a two steps method in a sequential manner was performed as control: after LB transfer from the Langmuir trough, the gold plate is then immersed in an electrochemical cell in 75/25 H<sub>2</sub>O/ACN and electrolyzed at + 0.85 V/SCE for 6 min. This procedure provides a much less interesting result, and we suspect that the Au-ODA<sub>LB</sub> is damaged during the immersion in the electrochemical cell. Indeed, AFM imaging performed after immersion in the electrochemical cell confirms the partial dewetting of the LB monolayer on the gold surface (data not shown).

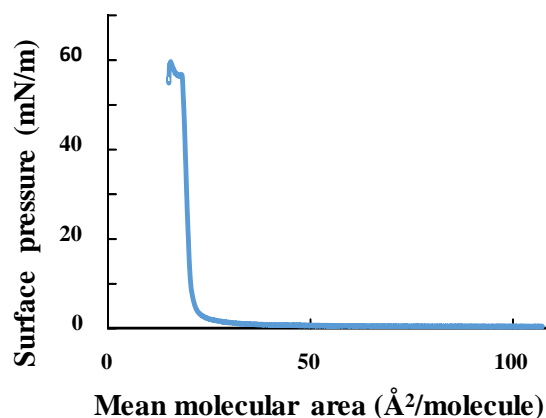


**Fig. 2:** Compression isotherm of ODA on pH 9 aqueous solution at 21°C.

The electrochemistry of primary amines has been investigated,<sup>32,57</sup> for example, *n*-butylamine is oxidized at + 1.36 V/SCE in DMF through a broad irreversible wave. In the same solvent, ODA (c = 1 mM) presents a small spread out wave E<sub>p</sub> = 1.36 V/SCE (Fig. SI-3). The onset of this wave is ~ 0.8 V/SCE. But as ODA is insoluble in a pH 9 aqueous solution, it is not possible to record the voltammogram and determine its oxidation potential under such conditions. On the other hand, the voltammogram of the same pH 9 solution used for the formation of Langmuir film presents background current starting at ~ 0.9 V/SCE (Fig. SI-4). Based on these data, we set the electrografting potential at + 0.85 V/SCE. Preliminary experiments performed by simply

depositing ODA on a gold electrode indicated that electrografting of ODA was possible at the potential of + 0.85 V/SCE.

The transferred, grafted and rinsed surfaces are examined by electrochemistry measurements, and characterized using water contact angle, ellipsometry, XPS, AFM, IRRAS and GIXD techniques in order to ascertain the presence and the organization of an ODA or ODOH film on the *Au* surface.

*Ultrasonication.* As a first control experiment, an *Au*-ODA<sub>LB</sub> film is submitted to a 3 min ultrasonication test. IRRAS spectra show that the *Au*-ODA<sub>LB</sub> is completely removed from the surface by this treatment (Fig. SI-6). As all films examined below have been sonicated under the same conditions, the IRRAS spectra cannot pertain to a remaining *Au*-ODA<sub>LB</sub> film adsorbed on the surface and correspond to strongly grafted *Au*-ODA<sub>LB-G</sub> film.

*Redox Probe.* The compacity of *Au*-ODA<sub>LB-G</sub> was tested with Fe(CN)<sub>6</sub><sup>3-/4-</sup> as a redox probe. This compound presents, in aqueous solution, a reversible voltammogram on an *Au* electrode at E = 0.21 V/SCE, but this voltammogram completely disappeared on *Au*-ODA<sub>LB-G</sub> (Fig. 3). This is interpreted as a blocking of the electrode by the grafted ODA film that is the electron transfer from the electrode to the inner sphere ferro/ferricyanide couple is impeded by the long alkyl chain attached to the *Au* surface.<sup>12</sup>

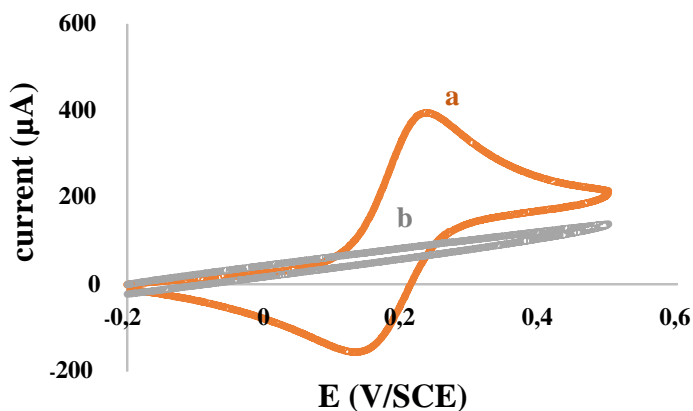


**Fig. 3.** Cyclic voltammetry of Fe (CN)<sub>6</sub><sup>3-/4-</sup> in aqueous solution +0.1 M KCl on a) *Au* and b) *Au*-ODA<sub>LB-G</sub>.  $v = 0.1 \text{ V.s}^{-1}$ .

*Thickness of the films.* The thickness of the  $Au\text{-ODA}_{\text{LB-G}}$ , and  $Au\text{-ODOH}_{\text{LB-G}}$  film were obtained by ellipsometry:  $1.69 \pm 0.3$  nm and  $1.51 \pm 0.4$  nm, respectively.

*Contact angle.* The water contact angle of  $Au\text{-ODA}_{\text{LB-G}}$  and  $Au\text{-ODOH}_{\text{LB-G}}$  films are respectively  $101.3^\circ \pm 0.5^\circ$  (Fig. SI-5) and  $95.7^\circ \pm 1.4^\circ$  as expected for long alkyl chains.

*XPS spectra.* The XPS of  $Au\text{-ODA}_{\text{LB-G}}$  (Table SI-1 and Fig. SI-9) survey spectrum indicates the presence of  $Au4f$  (9.52%) indicating that the film is thinner than 5-10 nm,  $C1s$  (70.76%),  $O1s$  (15.68%) and  $N1s$  (4.04%).  $O1s$  pertains to some contamination, but  $C1s$  is characteristic of the  $C_{18}$  carbon chain of ODA and the presence of  $N1s$  testifies from the presence of an ODA group on the  $Au$  surface. In addition, the ratio  $C1s / N1s$  is: 17.5 close to expected value of 18. The XPS spectra of  $Au\text{-ODOH}_{\text{LB-G}}$  (Table SI-2 and Fig. SI-11) are also in agreement with the expected structure.

*AFM images.* Fig. 4 shows AFM height (upper images) and phase (lower images) images of the  $Au$  surface before LB-eG process of ODA ( $5 \times 5 \mu\text{m}^2$ , left panel) and of  $Au\text{-ODA}_{\text{LB-G}}$  after ODA LB-eG process (at two different scales  $5 \times 5$  and  $2 \times 2 \mu\text{m}^2$ , central and right panels) (see Fig. SI-12 for  $Au\text{-ODOH}_{\text{LB-G}}$ ). The bare gold surface appears to be relatively flat at the nanometric scale (Figs 4A, 4D and 4G), with a mean roughness of 1.2 nm, and small gold spots observed all over the surface due to the evaporation process used to deposit the gold on the silicon surface.

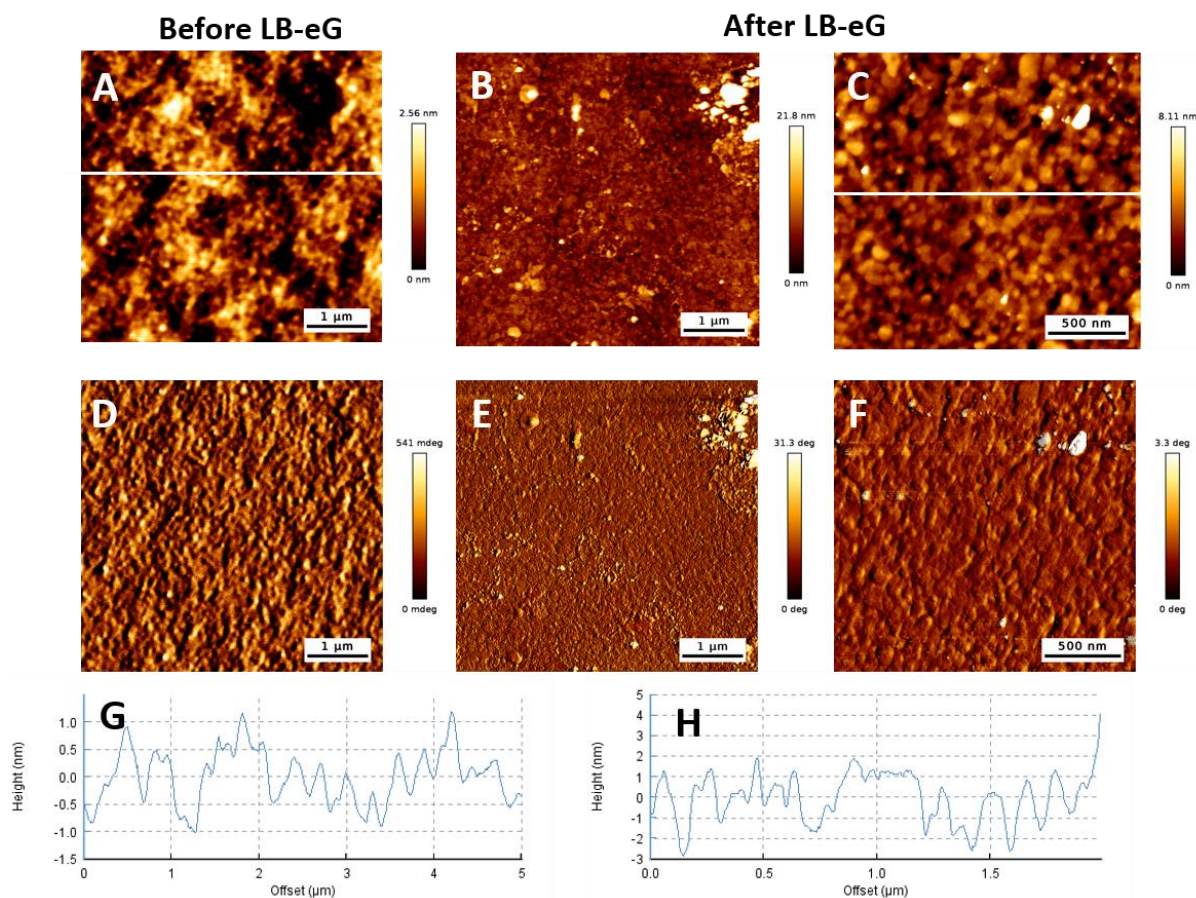


**Fig. 4:** AFM height pictures (A, B and C) and phase pictures (D, E and F) images of bare *Au* surface before LB-eG process of ODA (left panel) and of *Au-ODA*<sub>LB-G</sub> after ODA<sub>LB-eG</sub> process (central and right panels). Height cross sections G and H were performed along white lines drawn in images A (bare *Au* surface) and C (*Au-ODA*<sub>LB-G</sub>) respectively.

After LB-eG process of ODA on *Au*, we clearly distinguish a contrast change between the two images that confirms that we transferred and grafted a monolayer of ODA that covers the whole gold surface (Figs. 4B, 4E, 4C, 4F). Height profiles (Fig. 4H) demonstrate the presence of an ODA monolayer grafted onto the *Au* surface. An average height increase of about 2 nm is observed throughout the image that roughly corresponds to the thickness of an ODA monolayer. The mean surface roughness on picture 4C is 0.9 nm, corresponding to a decrease of 30% if compared to bare *Au* mean roughness and this is due to the ODA monolayer grafting that smoothens the surface. Height images indicate a complete coverage of the surface although very few pinholes of nanometric dimensions (2 nm depth and a few nanometers wide) can be observed in height images. Comparison of AFM images of films obtained by the simultaneous

LB-eG process with the sequential two steps method (not shown) indicates that the former method gives the best results in terms of monolayer quality.

*IRRAS Spectra.* In order to precise the structure of the grafted film, the IRRAS spectra of  $Au\text{-ODA}_{\text{LB-G}}$  (Fig. 5),  $Au\text{-ODOH}_{\text{LB-G}}$  (Fig. SI-13) can be compared (Table 1) with that of solids ( $\text{C}_{20}\text{H}_{42}$ , and ODA) and monolayer films ( $Au\text{-SC}_{18}\text{H}_{37}$  in Fig. 5 and ODA on mica), both with long alkyl chains; but also with disorganized structures such as liquid  $\text{C}_{18}\text{H}_{37}\text{SH}$ , long alkyl chains and ODA in solution. Table 1 presents the C-H stretching vibrations of these ordered and disorganized long alkyl chain structures. NH stretching appears as a sharp peak at  $3331\text{ cm}^{-1}$  (with two shoulders at  $3351$  and  $3259\text{ cm}^{-1}$ ) for solid ODA but as a broad strong peak at  $3249\text{ cm}^{-1}$  for  $Au\text{-ODA}_{\text{LB-G}}$ . The NH scissoring appears as weak bands at  $1567\text{ cm}^{-1}$  for solid ODA while it is located at  $1520\text{ cm}^{-1}$  for  $Au\text{-ODA}_{\text{LB}}$  and  $1590\text{ cm}^{-1}$  for ODA adsorbed as self-assembled monolayers (SAM) on mica<sup>58</sup>. This IR band is not observed for  $Au\text{-ODA}_{\text{LB-G}}$ . The same band is observed at  $1600\text{ cm}^{-1}$  for 4-nitrobenzylamine grafted on  $Pt$ ,<sup>32</sup> but cannot be safely assigned for  $Au\text{-ODA}_{\text{LB-G}}$ .

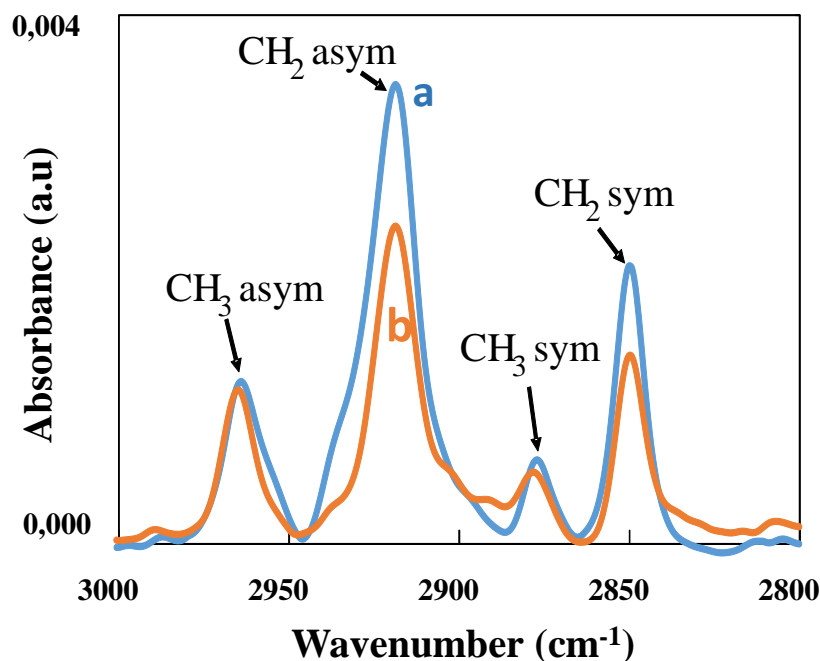


**Fig. 5:** IRRAS spectra of a)  $Au\text{-SC}_{18}\text{H}_{37}$  b)  $Au\text{-ODA}_{\text{LB-G}}$ .

**Table 1:** IRRAS spectra of  $Au\text{-ODA}_{\text{LB-G}}$  and other organized and disorganized long alkyl chains (wavenumbers in  $\text{cm}^{-1}$ ).

	$\text{CH}_3$ as	$\text{CH}_2$ as	$\text{CH}_3$ s	$\text{CH}_2$ s
Organized structures and films				
$Au\text{-SC}_{18}\text{H}_{37}$	2965	2917	2877	2850
$\text{C}_{20}\text{H}_{42}$ crystal <sup>59,60</sup>	2962	2914	2869	2850
ODA solid	2955	2917	2872	2850
ODA on mica <sup>58</sup>	2955	2917	2870	2850
$Au\text{-ODA}_{\text{LB}}$	2965	2917		2850
<b><math>Au\text{-ODA}_{\text{LB-G}}</math></b>	<b>2965</b>	<b>2917</b>	<b>2977</b>	<b>2850</b>
<b><math>Au\text{-ODOH}_{\text{LB-G}}</math><sup>a</sup></b>	<b>2965</b>	<b>2917</b>	<b>2878</b>	<b>2850</b>
Disordered structures				
$\text{HSC}_{18}\text{H}_{37}$ liquid		2924		2855
Polymethylene chains <sup>59,60</sup>		2928		2856
ODA in $\text{CCl}_4$ solution		2928		2855

<sup>a,b</sup> presents another band assigned to a Fermi resonance<sup>59</sup> at <sup>a</sup> 2939 and <sup>b</sup> 2935  $\text{cm}^{-1}$ .

*Comparison with electrografted ODA film.* In order to compare ODA films prepared using the LB-eG process to those prepared by grafting from a solution, samples of  $Au\text{-ODA}_{\text{G}}$  were prepared by grafting a solution of ODA in DMF. Samples were grafted either at + 0.85 V/SCE as for  $Au\text{-ODA}_{\text{LB-G}}$  or at + 1.40 V/SCE corresponding to the peak potential of ODA in DMF. The results are reported in Table 2.

**Table 2:** Ellipsometry, water contact angle and IRRAS characterizations of two electrografted ODA films from solution performed at two electrochemical potential values.

Grafting potential	Thickness of the film	Water contact angle	IRRAS spectra	
			CH <sub>2</sub> stretching	
+ 0.85 V/SCE (600s)	4.2 ± 1.8 nm	95.1 ± 0.9°	2926 cm <sup>-1</sup>	2856 cm <sup>-1</sup>
+ 1.40 V/SCE (600s)	5.0 ± 2.3 nm	89.6 ± 2.5°	2922 cm <sup>-1</sup>	2856 cm <sup>-1</sup>

The films obtained by electrografting from solution are multilayered as shown by thickness values; the higher the potential the thicker the film, their water contact angle is lower than that of *Au-LBODAG*. The corresponding IRRAS spectra of samples obtained at + 0.85 V/SCE show disorganized films. IR bands of the films obtained at + 1.4 V/SCE are located in-between an ordered and a disorganized film, probably due to a coexistence of organized and disorganized structures in the film.

*Grazing Incidence X-ray Diffraction experiments.* Monolayers of pure ODA formed on *Au* surface using the LB-eG process can generate a GIXD signal. Fig. 6 presents GIXD data obtained for ODA monolayer that was spread on water, compressed to 40 mN/m surface pressure, then LB transferred at this pressure while electrografting was performed at + 0.85 V/SCE simultaneously to the LB transfer (*Au-ODA<sub>LB-G</sub>*).

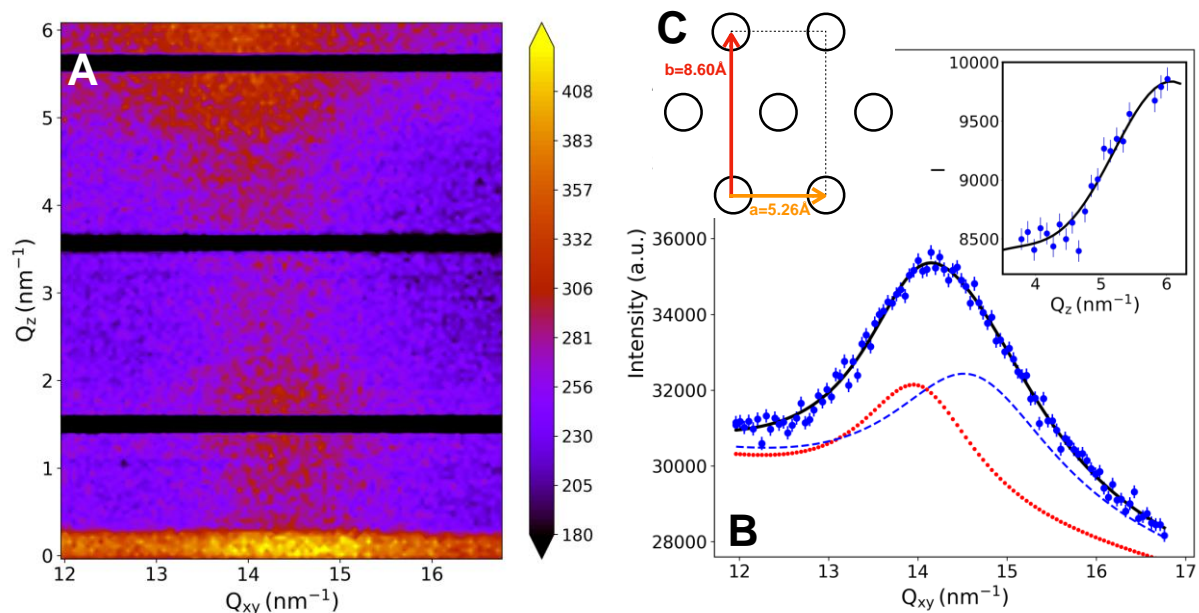


**Fig. 6:** GIXD intensity maps  $I(Q_{xy}, Q_z)$  obtained on  $Au\text{-ODA}_{\text{LB-G}}$  monolayer formed on  $Au$  using the LB-eG process (A). Fitting the curve  $I(Q_{xy})$  with Lorentzian peaks after integration along  $Q_z$  (B) reveals the in-plane positions of degenerated out-of-plane peaks indexed as  $[1\bar{1}]$  and  $[11]$  (red dotted line) and an in-plane peak  $[02]$  (blue dashed line). The intensity of the  $Q_{11}$  peak integrated along  $Q_z$  (Bragg rod) and the associated fit with a cardinal sine are shown in insert. The structure in real space as determined from the positions of the peaks is shown in C.

Data analysis yields two distinct diffraction peaks as shown in Fig. 6, one in-plane peak at  $Q_{xy} = 14.6 \text{ nm}^{-1}$ , and one degenerated out-of-plane peak at  $Q_{xy} = 14.0 \text{ nm}^{-1}$ ,  $Q_z = 6 \text{ nm}^{-1}$ . This corresponds to a rectangular structure of the chains with a tilt towards their nearest neighbors, with the out-of-plane peaks indexed as  $[11]$  and  $[1\bar{1}]$ , and the in-plane peak as  $[02]$ . The parameters of the rectangular cell as deduced from the position of the peaks are  $a = 5.26 \pm 0.10 \text{ \AA}$  and  $b = 8.60 \pm 0.30 \text{ \AA}$  (Fig. 6C). Analysis of the out-of-plane position of the  $[11]$  peak (inset in Fig. 6 B) is made difficult by its proximity to the border of the detector. Nevertheless, a fit with a sine cardinal function gives a peak position of  $Q_z = 6 \text{ nm}^{-1}$  indicating a tilt angle of the molecules of about  $30^\circ$  towards their nearest neighbors. The full width at half maximum of the in-plane Bragg peak (Fig. 6B) is of  $1.1 \text{ nm}^{-1}$  and corresponds to an in-plane correlation length of  $18 \text{ \AA}$ , indicating an ordering which extends up to the third nearest neighboring molecules. No diffraction peak was detected on  $Au\text{-ODOH}_{\text{LB-G}}$  monolayers at all.

## Discussion

*The film is different from an electrografted film directly obtained from solution.* Previous works reported the immobilization of organosilanes on glass or silicon dioxide by comparing the Langmuir Blodgett and chemisorption methods<sup>2,3</sup>. To our knowledge, our study is the first attempt to combine simultaneously Langmuir Blodgett technique of monolayer transfer and electrografting in order to obtain organized monolayer on metallic surfaces. Differences in thicknesses measured by ellipsometry and AFM, water contact angles and IR spectra between  $Au\text{-ODA}_{\text{LB-G}}$  and  $Au\text{-ODA}_{\text{G}}$  samples demonstrate that film structures are different on the gold surface. In particular, IR spectra demonstrate that disorganized structures are obtained by direct electrografting  $Au\text{-ODA}_{\text{G}}$  while ordered structures like thiols SAMs are obtained using the LB-eG process ( $Au\text{-ODA}_{\text{LB-G}}$ ).<sup>61</sup>

*The film is strongly grafted.* All results demonstrate that both  $Au\text{-ODA}_{\text{G}}$ <sup>32</sup> and  $Au\text{-ODA}_{\text{LB-G}}$  samples resist a 3 min ultrasonication rinsing step while the same treatment completely removes a LB-adsorbed  $Au\text{-ODA}_{\text{LB}}$  film. This test demonstrates that a covalent bond is effectively formed between the surface and the organic film.<sup>12,13</sup>

*The film is a monolayer with few pinholes.* Comparison between ellipsometry (1.69 nm) and AFM (2 nm) measurements and the length of a fully extended ODA molecule obtained from molecular models (2.32 nm) demonstrate the presence of a single ODA monolayer after LB-eG process. In addition, the redox probe experiment and the AFM pictures both demonstrate a compact monolayer: ODA covers the entire gold surface and smoothens it by decreasing the mean surface roughness. AFM pictures obtained at low scale demonstrate however the presence of few pinholes of 2 nm depth and a few nanometers wide in the  $Au\text{-ODA}_{\text{LB-G}}$  layer, suggesting that the monolayer is not fully continuous at the nanometric scale on gold surface. These features are probably due to the underlying  $Au$  surface roughness (1 nm).

*The film is “organized”.* The spectrum of  $Au\text{-SC}_{18}\text{H}_{37}$  was recorded (Fig. 5) as a reference. Thiols SAMs have been widely investigated because they provide ordered monolayers that are physisorbed but not chemisorbed as recently reported<sup>62</sup>. Their IR spectra<sup>63,64,65,66,67,68,69,70</sup> have been used to demonstrate the ordered structure. The spectrum of  $Au\text{-SC}_{18}\text{H}_{37}$  presents the  $\text{CH}_3$  and  $\text{CH}_2$  stretching vibrations at positions and absorbances that are identical to that of  $Au\text{-ODA}_{\text{LB-G}}$ ,  $Au\text{-ODOH}_{\text{LB-G}}$ . This result demonstrates that the LB film has been effectively transferred and grafted on gold. The  $\nu_s$  and  $\nu_{as}$  stretching of  $\text{CH}_2$  groups are located at 2850 and 2914-2917  $\text{cm}^{-1}$  for the crystalline state of  $\text{C}_{18}\text{H}_{37}\text{SH}$ , solid  $\text{C}_{20}\text{H}_{42}$ , solid ODA and  $Au\text{-ODA}_{\text{LB-G}}$

respectively, while they are observed at 2924-2928 and 2855-2856  $\text{cm}^{-1}$  for liquid  $\text{CH}_3(\text{CH}_2)_{15}\text{SH}$  and ODA in  $\text{CCl}_4$  solution (Table 1).<sup>71</sup> From these data we can deduce that  $\text{Au-ODA}_{\text{LB-G}}$  and  $\text{Au-ODOH}_{\text{LB-G}}$  are organized systems.

The tilt of the alkyl chains of thiols SAMs by reference to the surface normal has been deduced<sup>66</sup> from the intensity  $I$  of the alkyl stretching bands that is proportional to  $\cos^2 \Theta_{\text{mz}}$ , where  $\Theta_{\text{mz}}$  is the average angle between the transition dipole moments of the  $\text{CH}_2$  bonds ( $m$ ) and the surface normal ( $z$ ). The average tilt angle of the long alkyl chain was obtained as  $\alpha = 40^\circ$ . The same value is obtained for  $\text{Au-ODA}_{\text{LB-G}}$ , the chains are tilted by the same angle by reference to the surface normal. The tilt of the alkyl chain can also be obtained from the thickness of the film obtained by ellipsometry and the length of the molecule:  $43^\circ$ . These two values are in good agreement.

*The film possesses a short-range order.* GIXD measurements demonstrate that, after the LB-eG process, the  $\text{Au-ODA}_{\text{LB-G}}$  film is organized with a liquid order extending over  $18 \text{ \AA}$  that is up to the three nearest neighboring ODA molecules. This result has to be compared with the structure of both Langmuir and Langmuir-Blodgett ODA films using GIXD. Several studies reported the structure of ODA Langmuir films deposited on a pH 10 water subphase. Three distinct peaks were found at  $Q_{\text{xy}}$  positions 1.50, 1.53, and  $1.61 \text{ \AA}^{-1}$ , respectively indexed as  $(1\bar{1})$ ,  $(01)$ , and  $(10)$  respectively indicating an oblique hexagonal unit cell.<sup>16,19</sup> Ionov *et al.* studied the evolution of the main peak position  $(01)$  of ODA Langmuir film at pH 10 with increasing surface pressure. The position varies from  $1.47$  to  $1.52 \text{ \AA}^{-1}$ .<sup>72</sup> X-ray diffraction performed on ODA multilayered systems that were pre-formed by successive LB transfers, provides a lamellar spacing of  $5.2 \text{ nm}$ ,<sup>18</sup> a value twice larger than the ODA monolayer thickness measured by ellipsometry and AFM studies after the LB-eG process. Fenter *et al.* reported GIXD measurements of thiol monolayers of different length<sup>61</sup> and self-assembled on single crystal Au  $(111)$  surface. They showed that  $\text{CH}_3(\text{CH}_2)_{n-1}\text{SH}$  monolayers form expected  $\sqrt{3} \times \sqrt{3} R30^\circ$  structures with crystalline domains of  $90 \text{ \AA}$  size,<sup>61</sup> a value five times larger than that of  $\text{Au-ODA}_{\text{LB-G}}$  monolayer.

In our case, the obtained structure is a rectangular crystallographic cell for ODA on gold after the LB-eG process with cell parameters  $a = 5.26 \pm 0.10 \text{ \AA}$  and  $b = 8.60 \pm 0.30 \text{ \AA}$ . This structure is actually not very far from a hexagonal structure as depicted in Fig 6C. However, GIXD data could not be fitted with a purely hexagonal cell, because there are two diffraction peaks of

which one is out of the plane and degenerated (out-of-plane peaks indexed as  $[11]$  and  $[1\bar{1}\bar{1}]$ ). A rectangular crystallographic cell is therefore observed for ODA on gold with the LB-eG process, different from the hexagonal one observed with pure LB one<sup>19</sup>. This change in cell shape may be due to the organization of underlying gold atoms. The positions of the peaks are lower than those of ODA Langmuir film, indicating a larger spacing for ODA molecules after the LB-eG process and a lower crystalline order extension ( $18 \text{ \AA}$  which is up to the their third nearest neighboring molecules). As compared to ODA Langmuir film, this loss in order extension is of one order of magnitude. Thus,  $Au\text{-ODA}_{\text{LB-G}}$  monolayer organization is intermediate between the highly ordered ODA Langmuir film on water and the fully disorganized  $Au\text{-ODA}_{\text{G}}$  obtained from electrografting in solution. These results can be explained by the structure of the underlying gold surface as well as the grafting process.

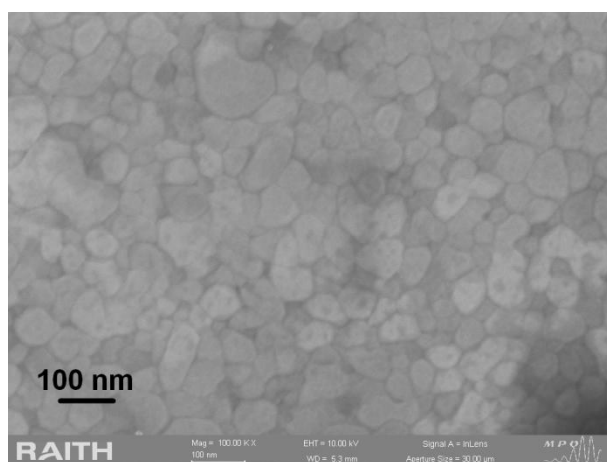


**Fig. 7:** Scanning electron microscopy picture obtained on bare  $Au$  surface used for LB-eG process and GIXD characterization.

Indeed, the gold surface we have used in this article is a polycrystalline  $Au$ , not a monocrystal one, since the unit cells are paired and form hyperdomains that are observed by STM<sup>73</sup>, or by scanning electron microscopy as shown in Fig. 7. Such polycrystalline  $Au$  surfaces are commonly used in biosensor applications. The domain size ranges between 20 and 50 nm. No correlation of orientation exists between the different domains. This lack of unique orientation at the gold surface impairs the preservation of ODA Langmuir film during the LB-eG process. Note also that the LB-eG process induces a grafting in dynamic conditions because of the LB transfer occurring at the  $Au$ /Langmuir film interface. The organization of ODA molecules on  $Au$  surface is therefore strongly dependent on that of underlying gold atoms. After the LB-eG

process, ODA molecules are bound to the gold surface *via* covalent bonds and cannot rearrange themselves as physisorbed ODA molecules do after a pure LB transfer or self-assembled thiol monolayers. Fig. 8 gives a schematic representation of the structure of the ODA film assuming that grafting occurs atop gold atoms (without bridged structures, as diazonium salts<sup>37</sup>).

$Au-ODOH_{LB-G}$  presents an IR spectrum that, by comparison with thiols SAMs, appear as organized, but no diffraction peak could be observed by GIXD, suggesting this layer is disorganized. It must be reminded that the observation of organized films by IRRAS is a purely experimental observation based on “the evolution of the adsorbates from a disordered phase of sub-monolayer at short deposition times, to the more ordered arrangement of butanethiol films following extended exposure to the thiol solution”.<sup>63</sup> The combination of IRRAS and GIXD is necessary to reveal the degree of order in the monolayer.

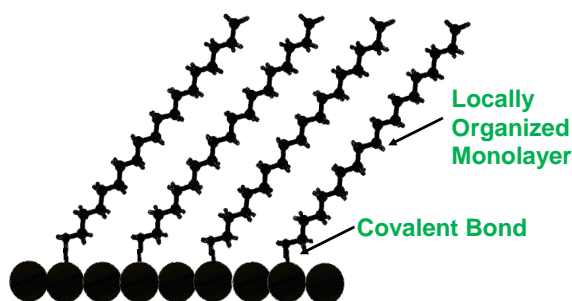


**Fig. 8:** A Schematic 2D representation of the locally organized electrografted LB film ( $Au-ODA_{LB-G}$ ) inside each domain of gold surface.

It would be worth to use monocrystalline  $Au$ , such as  $Au$  (111) surfaces, to perform LB-eG process to examine the extent of preservation of ODA Langmuir film after this grafting. However, such monocrystalline surfaces are difficult to produce, are less stable in air than polycrystalline ones, provided that the monocrystalline character of the surface remains unchanged during the LB-eG process.

## Conclusion

The simultaneous transfer of a LB film to a metallic electrode and *in situ* electrografting of this film permits to obtain, by construction, a locally ordered and strongly bonded monolayer with few nanometric pinholes. The film is characterized by various methods: electrochemistry, measurement of water contact angles, XPS, IR, AFM and GIXD. The structure of this film

consists in a strongly bonded ODA monolayer covering the whole surface. The ODA alkyl chains are tilted by the same angle ( $\sim 40^\circ$ ), but the film is characterized by a molecular ordering extending up to the three nearest neighboring molecules. This is due to the fact that the Au surface used is not a monocrystal but also to the covalent bonding that prevent molecules to rearrange on the surface. This LB-eG process provides an original method to obtain strongly grafted, locally ordered monolayers that can find applications in the field of sensors and biosensors.

**Acknowledgments.** The authors are grateful to Philippe Fontaine for GIXD studies on SIRIUS beamline at SOLEIL as well as fruitful discussions, to Philippe Decorse (ITODYS, Université de Paris) for XPS spectra and to Stephan Suffit (MPQ, Université de Paris) for the MEB images and for providing gold-coated wafers. They also thank SOLEIL synchrotron for providing beamtime on the SIRIUS beamline, MPQ lab for gold surfaces and access to instruments. The Institut Galien Paris Sud (IGPS, CNRS UMR 8612), ANR (Agence Nationale de la Recherche), CGI (Commissariat à l'Investissement d'Avenir) and the Région Ile de France are gratefully acknowledged for their financial support of this work, through Labex SEAM (Science and Engineering for Advanced Materials and devices) ANR 11 LABX 086, ANR 11 IDEX 05 02.

**Supporting information.** Image of the modified Langmuir trough. Electrografting of ODA on gold: electrochemical oxidation of ODA on gold, water contact angle on Au-ODA<sub>LB-G</sub>, infrared spectra of ODA solid, Au-SC<sub>18</sub>H<sub>37</sub>, Au-ODA<sub>LB-G</sub>, Au-ODOH<sub>LB-G</sub> and ODA<sub>LB</sub>, XPS of Au-ODA<sub>LB-G</sub>. Electrografting of ODOH on gold: water contact angle, XPS, AFM and IRRAS characterizations.

## Author information

### N°ORCID

Jean-Philippe Michel: [0000-0003-0242-2605](https://orcid.org/0000-0003-0242-2605)

Jean Pinson: [0000-0001-6176-8636](https://orcid.org/0000-0001-6176-8636)

Jérôme Médard: [0000-0002-4167-6336](https://orcid.org/0000-0002-4167-6336)

Arnaud Hemmerle: 0000-0003-1722-2024

## References

- 
- <sup>1</sup> K. B. Blodgett, *J. Am. Chem. Soc.*, 1935, **57**, 1007-1022.
- <sup>2</sup> A. Ulman, *Organic thin films: From Langmuir-Blodgett to self-assembly*, 1991, Academic Press, San Diego, USA
- <sup>3</sup> K. Kojio, A. Takahara, K. Omote, T. Kajiyama, *Langmuir* 2000, **16**, 3932.
- <sup>4</sup> C. Vericat, M. E. Vela, G. Benítez, P. Carro and R.C. Salvarezza, *Chem. Soc. Rev.*, 2010, **39**, 1805–1834.
- <sup>5</sup> E. Pensa, E. Cortès, G. Corthey, P. Carro, C. Vericat, M. H. Fonticelli, G. Benítez, A. A. Rubert and R.C. Salvarezza, *Acc. Chem. Res.*, 2012, **45**, 1183–1192.
- <sup>6</sup> S. P. Pujari, L. Scheres, A. T. M. Marcelis, and H. Zuilhof, *Angew. Chem. Int. Ed.*, 2014, **53**, 6322–6356.
- <sup>7</sup> J. Sagiv, *J. Am. Chem. Soc.* 1980, **102**, 92-98.
- <sup>8</sup> S. R. Wasserman, Y. T. Tao and G. M. Whitesides. *Langmuir* 1989, **5**, 1074-1087.
- <sup>9</sup> K. Ariga, Y. Okahata, *J. Am. Chem. Soc.* 1989, **111**, 5618- 5622
- <sup>10</sup> S. Ge, A. Takahara, T. Kajiyama, *J. Vac. Sci. Technol.* 1994, A12, 2530
- <sup>11</sup> C. Queffélec, M. Petit, P. Janvier, D. A. Knight and B. Bujoli, *Chem. Rev.*, 2012, **112**, 3777–3807.
- <sup>12</sup> A. Berisha, M. M. Chehimi, J. Pinson and F. I. Podvorica, F. I. *Electrode Surface Modification Using Diazonium Salts in Electroanalytical Chemistry*, Vol. 26 Eds A. J. Bard, C. G. Zoski, CRC Press: Boca Raton, FL, **2016**; 115–224.
- <sup>13</sup> M. M. Chehimi, *Aryl Diazonium Salts. New Coupling Agents in Polymer and Surface Science*, Wiley-VCH: Weinheim, Germany, **2012**.
- <sup>14</sup> J. P. Michel, Y. X. Wang, E. Dé, P. Fontaine, M. Goldmann and V. Rosilio, *Biochimica Biophysica Acta, Biomembranes*, 2015, **1848**, 2967-2979.
- <sup>15</sup> J. Daillant, A. Gibaud, *X-ray and neutron reflectivity: principles and applications*, Springer-Verlag: Berlin, **1999**.
- <sup>16</sup> V. M. Kaganer, H. Mohwald and P. Dutta, *Rev. Mod. Phys.*, 1999, **71**, 779-818.
- <sup>17</sup> I. Kuzmenko, *Chem. Rev.*, 2001, **101**, 1659-1696.
- <sup>18</sup> A. Angelova and R. Ionov, *Langmuir*, 1996, **12**, 5643-5653.

- 
- <sup>19</sup> N. Belman, S. Acharya, O. Konovalov, A. Vorobiev, J. Israelachvili, S. Efrima and Y. Golan, *Nano Lett.* 2008, **8**, 3858-3864.
- <sup>20</sup> S. W. Barton, A. Goudot, F. Rondelez. *Langmuir* 1991, **7**, 1029-1030.
- <sup>21</sup> K. Kojio, A. Takahara, K. Omote, T. Kajiyama, *Langmuir* 2000, **16**, 3932-3936.
- <sup>22</sup> K. Kjaer, J. Als-Nielsen, C. A. Helm, L. A. Laxhuber, H. Mohwald, *Phys. Rev. Lett.* 1987, **58**, 2224.
- <sup>23</sup> P. G. de Gennes, *Capillarity and Wetting Phenomena: Drops, Bubbles, Pearls, Waves*, Springer Editions, Berlin, **2003**.
- <sup>24</sup> A. Berisha, C. Combellas, F. Kanoufi, J. Médard, P. Decorse, C. Mangeney; I. Kherbouche, M. Seydou, F. Maurel and J. Pinson, *Langmuir*, 2018, **34**, 11264–11271.
- <sup>25</sup> C. A. Alves, E. L. Smith and M.D. Porter. *J. Am. Chem. Soc.*, 1992, **114**, 1222-1227.
- <sup>26</sup> K. Tamada, M. Hara, H. Sasabe and W. Knoll, *Langmuir*, 1997, **13**, 1558-1566.
- <sup>27</sup> E. Delamarche, B. Michel, H. A. Biebuyck and C. Gerber, *Adv. Mater.* 1996, **8**, 719-729.
- <sup>28</sup> K. Kjaer, J. Als-Nielsen, C. A. Helm, P. Tippman-Krayer, H. Mohwald, *J. Phys. Chem.* 1989, **93**, 3200
- <sup>29</sup> C. A. Helm, P. Tippmann-Krayer, H. Möhwald, J. Als-Nielsen, and K. Kjaer, *Biophys. J.* 1991, **60**, 1457-1476.
- <sup>30</sup> G. Brezesinski, F. Bringezu, G. Weidemann, P. B. Howes, K. Kjaer, and H. Möhwald, *Thin Solid Films*, 1998, **327-329**, 256-261.
- <sup>31</sup> D. Bélanger, and J. Pinson, *Chem. Soc. Rev.* 2011, **40**, 3995–4048.
- <sup>32</sup> A. Adenier, M. M. Chehimi, I. Gallardo, J. Pinson, and N. Vilà, *Langmuir*, 2004, **20**, 8243-8253.
- <sup>33</sup> V. Ramírez-Delgado, A. Méndez-Albores, A. Galano, and F. J. González, *Electrochim. Acta*, 2017, **245**, 472-481.
- <sup>34</sup> H. Maeda, M. Itami, Y. Yamauchi, and H. Ohmori, *Chem. Pharm. Bull.* 1996, **44**, 2294-2299.
- <sup>35</sup> D. Hetemi, J. Médard, P. Decorse, C. Combellas, F. Kanoufi, J. Pinson, and F. I. Podvorica, *Langmuir*, 2016, **32**, 6335–6342.
- <sup>36</sup> L. Koefoed, S. U. Pedersen and K. Daasbjerg, *Langmuir*, 2017, **33**, 3217–3222.
- <sup>37</sup> D.-e. Jiang, B. G. Sumpter and S. Dai, *J. Am. Chem. Soc.*, 2006, **128**, 6030–6031.
- <sup>38</sup> A. Berisha, C. Combellas, F. Kanoufi, P. Decorse, N. Oturan, J. Médard, M. Seydou, F. Maurel, and J. Pinson, *Langmuir*, 2017, **33**, 8730–8738.

- 
- <sup>39</sup> C. Combellas, D.-e. Jiang, F. Kanoufi, J. Pinson and F.I. Podvorica, *Langmuir*, 2009, **25**, 286-293.
- <sup>40</sup> Y. R. Leroux and P. Hapiot, *Chem.Mater.*, 2013, **25**, 489–495.
- <sup>41</sup> V. Malyskyi, L. Troian-Gautier, A. Mattiuzzi, S. Lambotte, B. Cornelio, C. Lagrost, and I. Jabin. *I. Eur. J. Org. Chem*, 2018, 6590–6595.
- <sup>42</sup> J. Greenwood, T. H. Phan, Y. Fujita, Z. Li, O. Ivasenko, W. Vanderlinden, H. Van Gorp, W. Frederickx, G. Lu, K. Tahara, Y. Tobe, H. L. Uji-i, S. F. L. Mertens and S. De Feyter, *ACS Nano*, 2015, **9**, 5520–5535.
- <sup>43</sup> L. T. Nielsen, K. H. Vase, M. Dong, F. Besenbacher, S. U. Pedersen and K.; Daasbjerg, *J. Am. Chem. Soc.*, 2007, **129**, 1888-1889.
- <sup>44</sup> O. Fontaine, J. Ghilane, P. Martin, J.-C. Lacroix, and H. Randriamahazaka, *Langmuir*, 2010, **26**, 18542–18549.
- <sup>45</sup> T. Menanteau, E. Levillain, T. Breton, *Chem.Mater.*, 2013, **25**, 2905–2909.
- <sup>46</sup> J. Ghilane, F. Hauquier and J.-C. Lacroix, *Anal. Chem.* 2013, **85**, 11593–11601.
- <sup>47</sup> J.-M. Chrétien, M. A. Ghanem, P. N. Bartlett and J. D. Kilburn, *Chem. Eur. J.*, 2008, **14**, 2548-2556.
- <sup>48</sup> H. Kang, S. Jung, S. Jeong, G. Kim and K. Lee, *Nature Comm.* 2015, **6**, 6503.
- <sup>49</sup> A. H. Holm, K. H. Vase, B. Winther-Jensen, S. U. Pedersen and K. Daasbjerg, *Electrochim. Acta* 2007, **53**, 1680–1688.
- <sup>50</sup> A. B. Bourlinos, D. Gournis, D. Petridis, T. Szabó, A. Szeri and I. Dékány, *Langmuir*, 2003, **19**, 6050-6055.
- <sup>51</sup> N. K. Chaki, and K. Vijayamohanan, *Biosensors Bioelectronics*, 2002, **17**, 1–12.
- <sup>52</sup> B. P. Corgier, C. A. Marquette and L. J. Blum, *J. Am. Chem. Soc.*, 2005, **127**, 18328-18332.
- <sup>53</sup> J. J. Gooding, *Electroanalysis* 2008, **20**, 573-582.
- <sup>54</sup> H. Maeda, Y. Yamauchi, M. Hosoe, T. X. Li, E. Yamaguchi, M. Kasamatsu, and H. Ohmori, *Chem. Pharm. Bull.* 1994, **42**, 1870-1873.
- <sup>55</sup> P. Fontaine, G. Ciatto, N. Aubert and M. Goldmann, *Sci. Adv. Mater.*, 2014, **6**, 2312-2316.
- <sup>56</sup> A. Guinier, *X-Ray Diffraction*, 1968, Freeman, San Francisco, Chap. 5.1.
- <sup>57</sup> J. L. Bourdelande, I. Gallardo, and G. Guirado, *J. Am Chem. Soc.*, 2007, **129**, 2817-2821.
- <sup>58</sup> J. J. Benítez, M. A. San-Miguel, S. Domínguez-Meister, J. A. Heredia-Guerrero, and M. Salmeron, *J. Phys. Chem., C* 2011, **115**, 19716–19723.

- 
- <sup>59</sup> R. G. Snyder and H. L. Strauss, *J. Phys. Chem.* 1982, 5145-5150.
- <sup>60</sup> R. A. MacPhai, H. L. Strauss, R. G. Snyder and C. A. Elliger, *J. Phys. Chem.*, 1984, **88**, 334-341.
- <sup>61</sup> P. Fenter, P. Eisenberg and K. S. Liang, *Phys. Rev. Lett.*, 1993, **70**, 2447-2450.
- <sup>62</sup> M. S. Inkpen, Z. F. Liu, H. Li, L. M. Campos, J. B. Neaton and L. Venkataraman, *Nature Chemistry*, 2019, **11**, 351–358.
- <sup>63</sup> K. D. Truong and P. A. Rowntree *Progress in Surface Science*. 1995, **50**, 207-216.
- <sup>64</sup> M. D. Porter, T. B. Bright, D. L. Allara and C. E. D. Chidsey, *J. Am. Chem. Soc.*, 1987, **109**, 3559-3568.
- <sup>65</sup> R. G. Nuzzo, E. M. Korenic and L. H. Dubois, *J. Chem. Phys.*, 1990, **93**, 767-773.
- <sup>66</sup> R. G. Nuzzo, L. H. Dubois and D. L. Allara, *J. Am. Chem. Soc.*, 1990, **112**, 558-569.
- <sup>67</sup> R. H. Terrill, T. A. Tanzer and P. W. Bohn, *Langmuir* 1998, **14**, 845-854.
- <sup>68</sup> F. Bensebaa and T. H. Ellis, *Langmuir*, 1998, **14**, 2361-2367.
- <sup>69</sup> F. Tielens, D. Costa, V. Humblot and C. M. Pradier, *J. Phys. Chem., C* 2008, **112**, 182-190.
- <sup>70</sup> Ž. Ruželá, L. Malysheva, A. Onipko, A. Gutés, F. Björefors, R. Valiokas and B. Liedberg, *Langmuir*, 2009, **25**, 13959–13971.
- <sup>71</sup> H. Yeon, C. Wang, R. C. Van Lehn and N. L. Abbott, *Langmuir* 2017, **33**, 4628–4637.
- <sup>72</sup> R. Ionov, A. El-Abed, M. Goldmann, P. Perreti, *Biochim Biophysica Acta*. 2004, **1667**, 200-207.
- <sup>73</sup> G. E. Poirier, *Chem. Rev.*, 1997, **97**, 1117–1127.

TOC graphic

